Frequency Support Comparison for Vanadium and Lithium-ion BESSs Using a Converter-based Grid Emulator

Jessica D. Boles[1,2], Yiwei Ma[1], Leon M. Tolbert[1,3], and Fred Wang[1,3]

[1]The University of Tennessee, Knoxville, Tennessee, USA, 37996
[2]Massachusetts Institute of Technology, Cambridge, Massachusetts, USA, 02139
[3]Oak Ridge National Laboratory, Oak Ridge, Tennessee, USA, 37831

***Abstract*—Battery energy storage systems (BESSs) are commonly used for frequency support services in power systems because they have fast response times and can frequently inject and absorb active power. Lithium-ion (Li-ion) BESSs dominate the grid energy storage market now, but Vanadium redox flow (VRB) BESSs are predicted to contend in future markets for large-scale storage systems. Previously, a Li-ion BESS emulator has been developed for a grid emulation system known as the Hardware Testbed (HTB), which consists of converters controlled to emulate different power system components. In this paper, we develop a VRB BESS emulator with a VRB-specific internal battery model and a power electronics interface similar to that of the Li-ion BESS emulator. Then, we compare the effectiveness of the VRB and Li-ion technologies for primary frequency regulation and inertia emulation applications. It is concluded that these two technologies are virtually indistinguishable from the power system's perspective when conducting these services over a short period of time.**

I. Introduction

Energy storage decouples generation and load in a power system by shifting power delivery across time. When used strategically, it can provide several benefits to the grid such as increased reliability, increased generation efficiency, better integration of renewable energy sources, and deferral of infrastructure investments [1]–[3]. A plethora of applications exists for energy storage in power systems, and each requires a certain storage capacity and power rating to be effective. Fig. 1 provides a visual comparison of the power ratings and energy capacities for several energy storage technologies [1], [4]–[7].

As shown in Fig. 1, battery energy storage systems (BESSs) have the power range and capacity requirements to perform a variety of services related to power balancing, transmission and distribution (T&D), power quality, and reliability. They have become significantly more popular for grid applications in recent years due to their versatility, modularity, fast response times, high energy densities, and high efficiencies [2], [9]. More than 90% of new storage installations in the United States for every fiscal quarter since the end of 2014 have been Lithium-ion (Li-ion) BESSs [10], which are commonly used for frequency support applications. Li-ion BESSs are the most popular grid energy storage technology for new installations at this time due to their high power and energy densities, high efficiencies, and low self-discharge rates [1], [3]–[7], [11]–[13].

Flow batteries are different from conventional battery types in that their electrolyte solutions contain one or both of the battery's active materials. One unique advantage of flow batteries is the independence of their power and energy ratings due to external storage of their electrolytes (and active materials) [1], [5], [11], [12]. The most mature flow battery technology is the vanadium redox battery (VRB), which utilizes the reduction and oxidation of vanadium. Most of the new non-Li-ion energy storage capacity installed in 2017 has consisted of VRB systems, and these BESSs are projected to contend in future markets for large-scale grid storage [2], [4]–[6], [10], [11].

BESSs are capable of frequent cycling and have faster response times than conventional power plants, which make them prime candidates for providing grid frequency support [13]–[20]. The frequency of a power system deviates from its nominal value when an imbalance between generation and load arises, and frequency regulation compensates for short-lived imbalances so that the frequency stays at its nominal or scheduled value [21]. Synchronous generators can provide

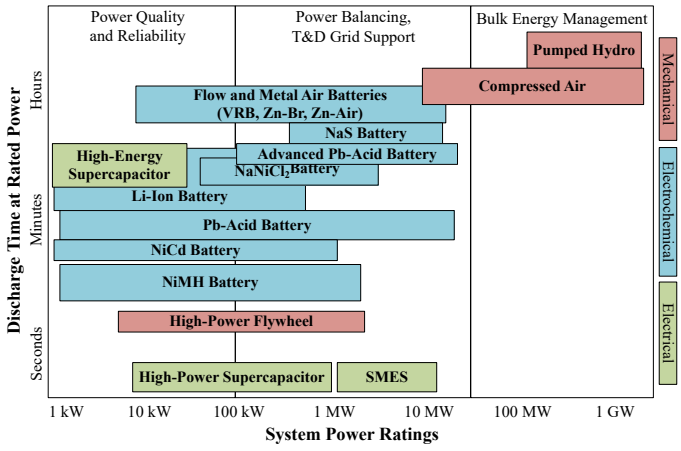

Fig. 1. Comparison of energy storage technologies in terms of power rating and capacity (discharge time at rated power) [1], [4]–[8].

regulating services by varying power output, but this causes them to degrade more quickly and requires deviation from their optimal operating points. Energy storage can provide frequency regulation more freely since it operates independently of generation, has faster response times, and has the ability to either inject or absorb power [5], [11], [12].

Primary frequency regulation (PFR) is the first reaction to system frequency changes and begins within seconds of a disturbance. Its purpose is to momentarily stabilize the frequency by filling the discrepancy between generation and load, but it does not return the frequency to its nominal value. It reacts in shorter time periods to system needs than other levels of frequency regulation, which is particularly important for sudden loss of generation or transmission lines [11], [12], [14], [21]. PFR is typically conducted using proportional control, so the power output of bodies conducting this service is directly proportional to the error in frequency [14].

The rate at which frequency changes in a power system as a result of power imbalance is directly proportional to the system's aggregate inertia. This inertia is determined by rotating masses in the system such as synchronous generators, and high amounts of inertia slow the rate of change of frequency during a disturbance and therefore allow more time for correction before system stability is lost [11], [12], [22]. Renewable sources such as wind and PV are tied to power systems with converters, which decouple generator motion from grid frequency. Thus, they contribute little or no inertia to the system, so replacing traditional generation with renewables leads to lower system-wide inertial response [22], [23]. Fortunately, energy storage and reserves can be controlled to mimic inertial response and other synchronous generator characteristics. This inertia emulation (IE) is typically realized through combined derivative and proportional control [13], [17], [18], [22], [23].

In [8], [24], converter-based Li-ion and Lead Acid BESS emulators were developed for frequency and voltage support applications on a power grid emulator referred to as the Hardware Testbed (HTB). The HTB consists of voltage source inverters controlled to emulate the dynamic behaviors at the terminals of various power system components [25]–[31]. Dynamic models for these power system components are implemented on digital signal processors (DSPs), which then each control a single inverter. When these inverters are arranged into a representative grid configuration on the HTB as shown in Fig. 2, the system emulates the behavior of a realistic power system. The inverters are easily reconfigurable, so this setup provides both the effectiveness of physical experiments and the flexibility of digital simulations [28].

Hardware emulation brings several benefits to experimental settings, namely added flexibility and reduced cost. Previous converter-based battery emulators have been developed primarily for electric vehicle applications [32]–[35] but not yet for grid applications outside of the HTB. This work documents the development of a VRB BESS emulator similar to the Li-ion emulator in [24] so that the two battery technologies can be compared for frequency support effectiveness on the HTB.

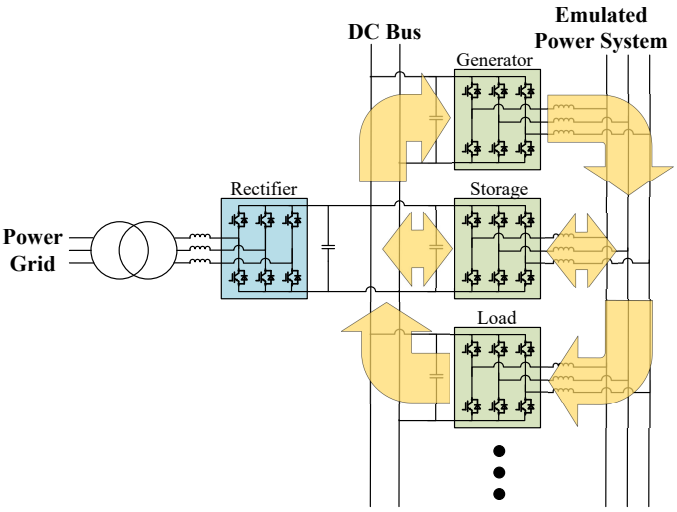

Fig. 2. Power circulation within the HTB [8].

By emulating nearly-identical Li-ion and VRB BESSs for the same grid conditions on the HTB, we can make a direction comparison between their frequency support capabilities.

II. VRB Internal Battery Model

There are several factors that contribute to the dynamic behavior of a battery. The open-circuit voltage of a battery changes nonlinearly as its SOC changes, and when a step change in load occurs, the battery's voltage exhibits a transient response with multiple time constants. This response is due to charge depletion and recovery, in which concentrated reactants disperse away from the electrodes when current begins and diffuse back to the electrodes when current ends, respectively. Model selection depends on the fidelity needed for the specific battery characteristics that are relevant to the application [36].

Electrical battery models tend to provide a practical trade-off between accuracy and complexity, especially for terminal electrical behavior. The simplest Thevenin electrical models use a constant open-circuit voltage, a constant equivalent series resistance, and an R-C network to model the battery's response to transients at a particular SOC as shown in Fig. 3 [32], [34], [36]–[40]. Adding additional R-C pairs increases accuracy, but typically only one or two are necessary. This model is only applicable for one SOC level, so its accuracy can be increased if dependence on SOC is added to each parameter.

The HTB is designed for studying short-term dynamic behaviors of power systems, so a Thevenin electrical model that provides the VRB's voltage time constant with a single R-C pair was selected for the VRB emulator's internal battery model. The model in [39] proposes the circuit topology shown in Fig. 3 for a 15-cell, 1 kW / 1 kWh VRB BESS. In addition to static and dynamic behavior, this model considers shunt current, self-discharge due to diffusion, and a hydraulic circuit model for pumping system losses. The open-circuit voltage (E_{ocv}) in this model is calculated as a function of standard electrode potential (E_o), the gas constant (G), the

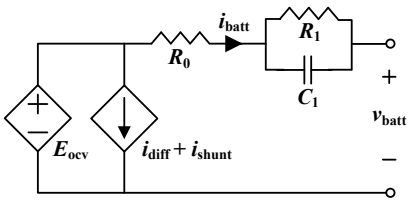

Fig. 3. Thevenin electrical model for VRB system [39].

Faraday constant (F), temperature (T), the apparent cell SOC (SOC_{cell}), and a curve-fitting coefficient (a) that accounts for differences in actual SOC and SOC calculation [39].

$$E_{ocv} = E_o + a\frac{2GT}{F}ln(\frac{SOC_{cell}}{1 - SOC_{cell}}) \quad (1)$$

The tank SOC (SOC_{tank}) is a direct measure of vanadium ion concentration level in the electrolyte tanks, and it changes as electrons move through the cell stack. Thus, it can be calculated as a function of F, tank volume (W), and the concentration of vanadium ions in the electrolyte (c). SOC_{cell} is related to SOC_{tank} but is also dependent on the electrolyte flow rate (U).

$$SOC_{tank} = SOC_{tank}(0) - \frac{15}{FWc}\int_0^t (i_{batt} + i_{diff})dz \quad (2)$$

$$SOC_{cell} = SOC_{tank} - \frac{15}{2FUc}(i_{batt} + i_{diff}) \quad (3)$$

The diffusion current is the following, where the self-discharge loss (η_{diff}) is 5%:

$$i_{diff} = \frac{\eta_{diff}}{2 - \eta diff}|i_{batt}| \quad (4)$$

Several sets of parameters for the VRB model are displayed in Table I [39], and the values for a terminal current density of 160 mA/cm^2 and an electrolyte flow rate of 4 L/min were used in the VRB emulator. Pumping system considerations were deemed unnecessary for short term electrical emulation and were therefore not included.

TABLE I
VRB INTERNAL MODEL PARAMETERS [39]

i_{batt} (A)	U (L/min)	a	R_0 (Ω)	R_1 (Ω)	C_1 (F)
124.8	2	1.6999	0.0209	0.0085	1.16e3
124.8	4	1.4537	0.0217	0.0031	1.90e3
124.8	6	1.3364	0.0218	0.0013	4.48e3
62.4	2	1.3203	0.0222	0.0098	1.34e3
62.4	4	1.2534	0.0247	0.0044	3.77e3
62.4	6	1.2176	0.0252	0.0019	6.57e3
-62.4	2	1.3461	0.007	0.0152	1.77e3
-62.4	4	1.2738	0.0102	0.0089	2.84e3
-62.4	6	1.2471	0.0103	0.0065	4.42e3
-124.8	2	1.5531	0.0107	0.0137	1.61e3
-124.8	4	1.3921	0.0104	0.0097	1.11e3
-124.8	6	1.3491	0.0102	0.0084	1.65e3

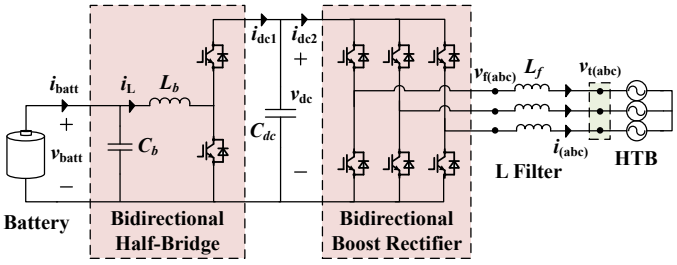

Fig. 4. Power electronics interface for emulated VRB and Li-ion BESSs [8].

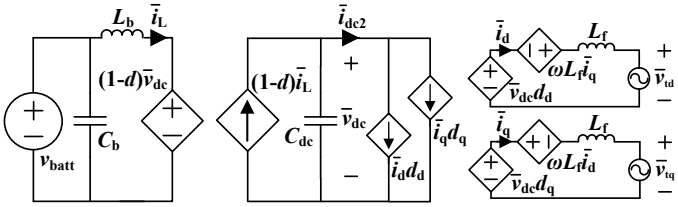

Fig. 5. Average electrical model of emulated VRB and Li-ion BESSs [8].

III. VRB INTERFACE MODEL AND CONTROL

For comparison purposes, the same power electronics interface used for the Li-ion BESS emulator in [24] was implemented for the VRB BESS emulator. This interface contains a bidirectional half-bridge and a bidirectional boost rectifier, separated by a DC link. The complete emulated BESS interface is shown in Fig. 4, and its average model is shown in Fig. 5.

The double-stage converter topology was selected for this application since having two stages allows for decoupled active and reactive power control. Also, since the boost rectifier on the emulated BESS has the same physical topology as the inverter on the HTB, the control references generated for the boost rectifier can be fed directly to the HTB inverter so that the inverter's terminal behavior emulates that of the BESS. Fig. 6 visualizes how the BESS model and the physical HTB inverter are integrated according to this strategy.

The HTB inverters are controlled in the synchronous dq domain, and all current-controlled emulators use the same inner current control loop for their inverters. The direct and quadrature current references for the BESS emulator are generated using its boost rectifier's DC link voltage control and reactive power control loops, respectively, as shown in Fig. 7. Active power control is conducted by the BESS half-bridge using inductor current control, which adopts constant power and constant current approaches for discharging and charging, respectively. The inductor current reference is calculated based on an active power reference input and the internal battery model. The reactive power control operates based on a reactive power reference input. The control parameters for each of these loops is shown in Table II.

Application-specific control loops for PFR, IE, and voltage support have been implemented for the Li-ion BESS emulator in [8], [24]. These outer control loops generate active and reactive power commands for the BESS emulator based on

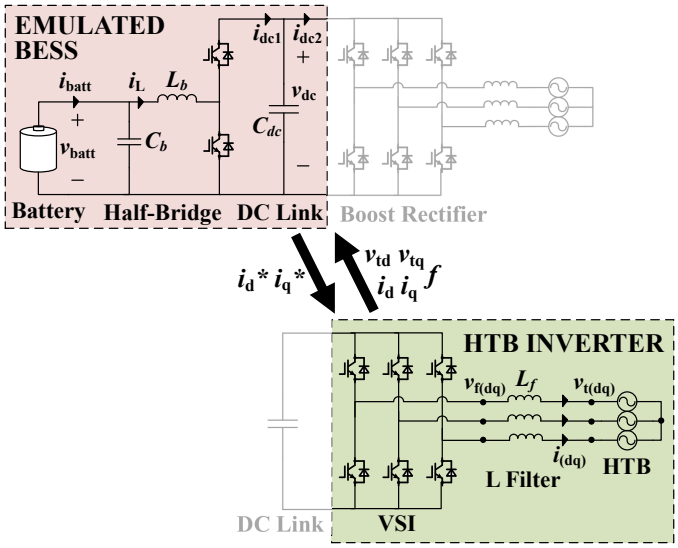

Fig. 6. Integration of the emulated BESS and a physical inverter on the HTB [8].

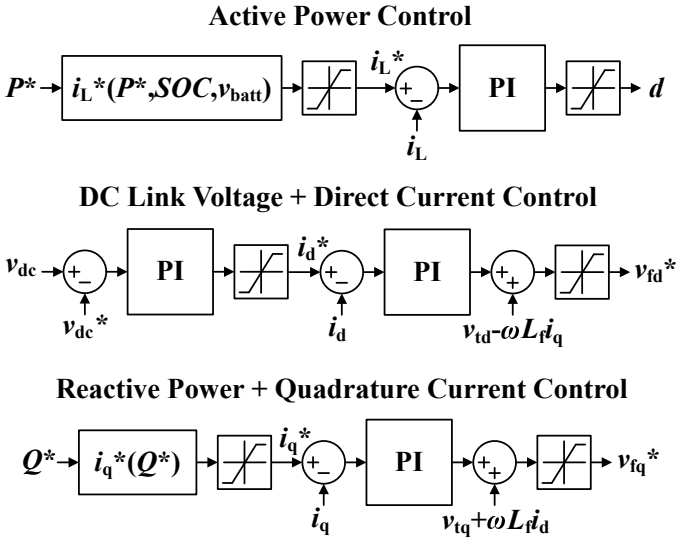

Fig. 7. Active power, DC link voltage, and reactive power control loops for emulated VRB and Li-ion BESSs [24].

power system frequency and voltage conditions, respectively. The PFR and IE control loop is shown in Fig. 8. Because this loop controls the active power command, internal battery characteristics play a role in the frequency control's performance.

The BESS emulator provides PFR with only the proportional control part of Fig. 8 enabled. This control loop generates the active power command for the BESS emulator based on system frequency needs. Like typical frequency regulation, a deadband of ± 10 mHz is implemented so the BESS does not operate constantly for small fluctuations. The deadband also includes a hysteretic characteristic so that PFR does not end until the frequency returns to within 8 mHz of its nominal value. This prevents the frequency from hovering around either the upper or lower deadband and forcing the BESS to work more frequently than necessary.

The BESS emulator conducts IE using the derivative part of the control loop in Fig. 8 so that its active power output reacts according to the frequency's rate of change. Derivative controllers are sensitive to input signal noise, so an additional low-pass filter was added after the calculation of the frequency error difference. The derivative controller contains a threshold so that it does not operate until it detects a frequency change of more than 0.6 Hz/s. When this threshold is met, the derivative controller operates for 10 seconds and then returns to its dormant state until it detects another frequency change above the threshold. When PFR and IE operate simultaneously, the output power command is a sum of their control outputs as shown in Fig. 8.

TABLE II
PARAMETERS FOR BESS EMULATOR CONTROL LOOPS

Control Loop	P	I	D
DC Link Voltage Control	3.1	304	–
Active Power Control	0.0015	0.0025	–
Frequency Control	0.01	–	0.1

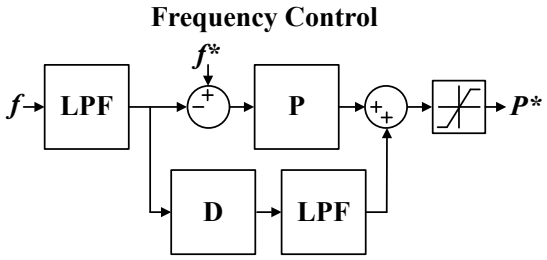

Fig. 8. Frequency control for emulated VRB and Li-ion BESSs, consisting of PFR and IE [8].

IV. IMPLEMENTATION

Because the emulator uses a simple double-stage power conditioning system, the BESS to be emulated was divided into parallel power blocks, each with the topology shown in Fig. 4. Each power block was rated at 1 MW and was assumed to connect to 480 V lines in the distribution system. Thus, the DC link voltage was designed to be 900 V, and the battery storage modules were arranged so that the nominal battery bus voltage is between 600 and 700 V. With this structure, the current references for the HTB inverter are multiplied by the number of these parallel power blocks required to achieve the desired BESS system capacity. Like the Li-ion emulator in [8], the VRB emulator was sized at 0.07 per unit (pu) power on the HTB's system. All models within the VRB emulator were converted to discrete equations using the Euler Method. For experimental testing, the final emulator control was implemented on a digital signal processor (DSP) that controls an inverter on the HTB.

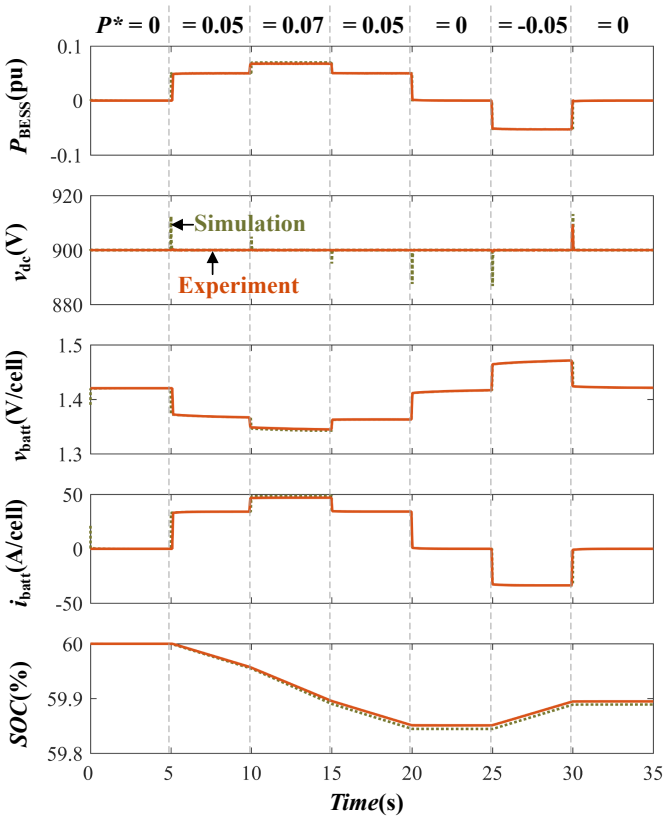

Fig. 9. Simulated and experimental waveforms for VRB BESS emulator active power control testing [8].

V. Simulation

The internal battery model along with the various control methods were first simulated in Matlab/Simulink to confirm appropriate behavior before experimental testing. The specifications and ratings outlined in the previous section were implemented in the emulated BESS model. The model's active power control capability was simulated using a series of active power command changes every five seconds from 0→0.05→0.07→0.05→0→-0.05→0 pu. The resulting waveforms are shown as the dotted line in Fig. 9.

Throughout the duration of this testing, the DC link voltage control kept the DC voltage within 1.5% of 900 V. As the battery discharged and charged, the SOC fell with a slope dependent on the input/output power level, which was highest when the active power command was 0.07 pu. As the cell current increased, the battery's voltage decreased due to internal series resistance. The specific cell voltage drop and SOC rate of change as a result of cell current were verified to match the published waveforms accompanying the VRB models in [39]. This appropriate response indicates correct implementation of the VRB BESS's internal battery model since that is the only component that differs from the Li-ion emulator verified in [8], [24].

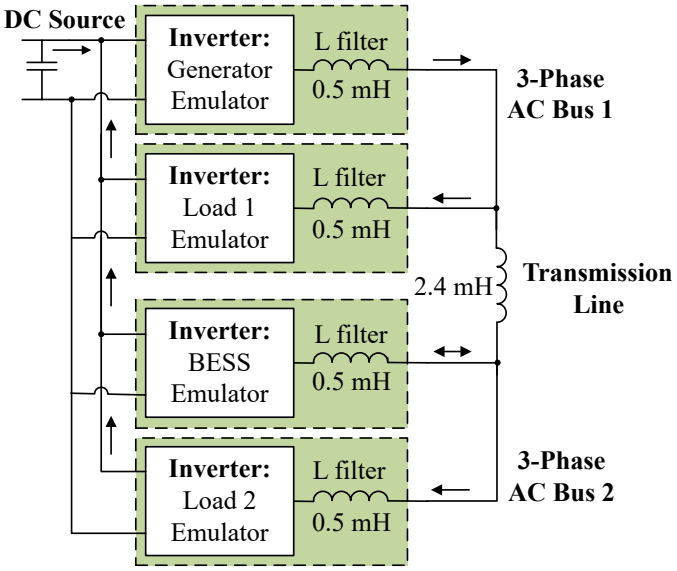

Fig. 10. HTB experimental setup for testing VRB and Li-ion BESS emulators [8].

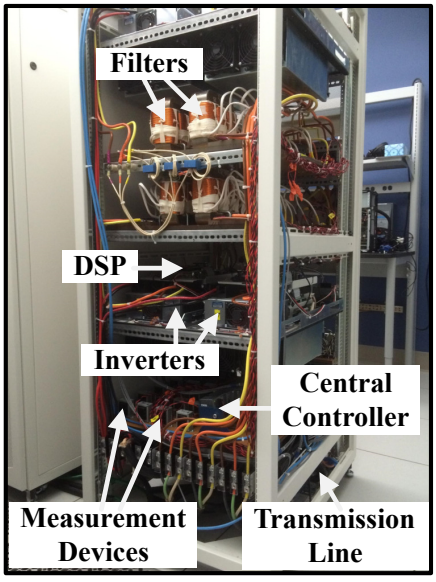

Fig. 11. Photo of HTB experimental setup [24].

VI. Hardware Emulation

The same experimental setup used for the Li-ion BESS emulator in [8] was used for testing the VRB BESS emulator so a direct comparison could be made between the two. Fig. 10 shows a diagram of this setup, which contains four inverters on the HTB arranged into two buses, separated by a 2.4 mH transmission line. Each inverter has a 0.5 mH inductor filter at its AC terminal. One of these inverters was controlled to emulate a synchronous generator, one on each bus was controlled to emulate a constant power load, and one was controlled to emulate the VRB BESS. With this setup, generating emulators convert power from DC to AC, and load

emulators convert power from AC to DC, so power circulates within the structure and the AC side represents the emulated power system. A photograph of the setup is shown in Fig. 11.

Like in simulation, the BESS emulator was set to have a capacity of 0.07 pu on the current HTB system design. The VRB BESS emulator's active power control was tested first with the same command sequence used for simulation, and the resulting waveforms are overlaid in orange on top of the simulated waveform in Fig. 9. Both waveforms show a similar step-change response in active power output, and the emulated VRB BESS shows DC link regulation to within 1% of 900 V. The average cell voltage waveform shows appropriate decreases when power output increases and the same in reverse due to internal series resistance. Also, the SOC level decreases during discharging and increases during charging at a rate dependent on power input/output.

The primary difference between the simulated and experimental active power control tests were disturbances in the DC link voltage, which appear to be significantly smaller in the experimental results. This can be attributed to the fact that the simulation records data points every 100 μs but the experimental data only has a precision of 100 ms. Since the DC link voltage spike observed in the simulation occurs for very little time, it is likely that its highest points are missed by the experimental data collection. Otherwise, the experimental waveforms were nearly identical to the simulated waveforms, so the emulator was concluded to function correctly in response to the active power commands.

The generator and load emulators were brought to the operating points specified in Table III. For generators and storage on the HTB, a positive power value indicates power injection and a negative power value indicates absorption. For loads, a positive power value refers to absorption and a negative value indicates injection.

The VRB BESS emulators effectiveness at conducting PFR and IE was tested using on-off step changes in Load 1 every 20 seconds. First, only the PFR was enabled, and the resulting waveforms are shown in Fig. 12. Because the PFR consists of only proportional control, the BESS emulator's active power output tracked the frequency's deviation from 60 Hz when it left its deadband of $\pm$10 mHz. In this case, the frequency settled closer to 60 Hz when the load was off but further from it when the load was on, so the amount of active power provided varied accordingly. In response to the load changes, the frequency's peaks and nadirs were significantly reduced with the PFR when compared to the case without it as shown in Table IV.

Then, the BESS emulator's IE function was enabled in

TABLE III
OPERATING POINT OF EMULATORS IN HTB EXPERIMENTAL SETUP

Power	Generator	Load 1	Load 2
P_{mech} (pu)	0.1	–	–
P (pu)	–	0.1	0.07
Q (pu)	–	-0.1	-0.1

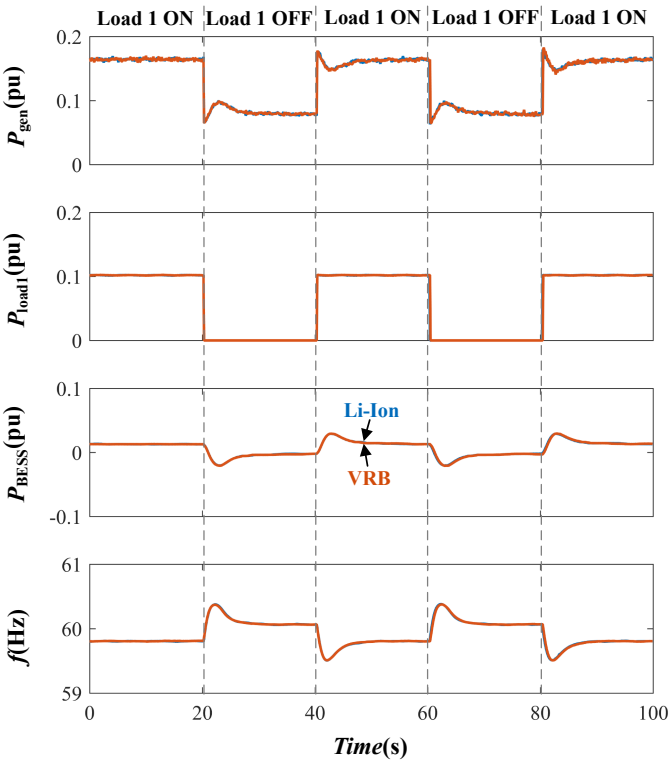

Fig. 12. Experimental waveform comparison of VRB and Li-ion BESS emulators conducting PFR [8].

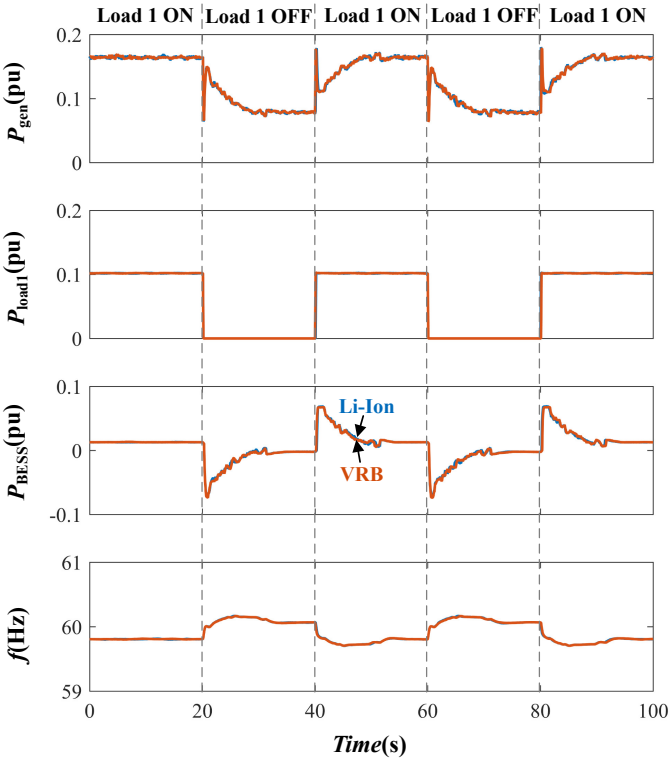

Fig. 13. Experimental waveform comparison of VRB and Li-ion BESS emulators conducting PFR and IE [8].

TABLE IV
AVERAGE FREQUENCY EXTREMA RESULTING FROM EMULATED VRB AND LI-ION BESS FREQUENCY SUPPORT SERVICES

Extremum	None	PFR (VRB)	PFR (Li-ion)	PFR+IE (VRB)	PFR+IE (Li-ion)
Peak (Hz)	60.667	60.374	60.379	60.165	60.166
Nadir (Hz)	59.364	59.509	59.509	59.705	59.704

addition to the PFR. The system was cycled through the same load changes every 20 seconds, and the resulting waveforms are shown in Fig. 13. With the IE enabled, the frequency control reacted very quickly and forced the emulated BESS to reach full power almost immediately once the frequency change was detected. It then gradually declined in power input/output, resulting in a similarly-slow power curve for the generator that resembles a heavy inertial response. As a result, the frequency ultimately ramped to its new stable value instead of swinging, which is significantly less taxing on the system as a whole. It is clear that adding only the PFR helps suppress the frequency transient and reduces the duration of its swing, but the best response is achieved when IE is also enabled as apparent in Table IV.

The waveforms for both of these VRB BESS frequency control tests were compared with identical tests using the Li-ion BESS. Figs. 12 and 13 contain the VRB emulator waveforms superimposed on the Li-ion emulator waveforms. These waveforms, along with the frequency peaks and nadirs reported in Table IV, show that the emulated VRB and Li-ion BESSs behave nearly identically when conducting frequency support services.

VII. VRB AND LI-ION BESS COMPARISON

As shown in hardware emulation, the Li-ion and VRB BESSs behave very similarly and are nearly indistinguishable from the power system's perspective. Their waveforms in Figs. 12 and 13 are almost exactly the same, and the resulting peak frequency deviations in Table IV are within 1.4% of each other for both types of frequency support. This can be attributed to the fact that the VRB and Li-ion cell-level differences are effectively decoupled from the power system by the two-stage power electronics interface. The dynamics of both systems are slow enough for the power electronics to track them and keep the desired power output, so they are not observable at the system level.

Thus, for power system frequency support services, either technology can be used, and the choice between them should depend on other technical specifications and economics rather than frequency support performance from the power system's perspective.

VIII. CONCLUSION

A converter-based VRB BESS emulator has been developed for use with power system hardware emulation, and its frequency support capabilities have been compared with those of a similarly emulated Li-ion BESS. Experimental results demonstrate that the emulated VRB and Li-ion BESSs provide virtually the same system-level efficacy for PFR and IE support functions. This can be attributed to the fact that the batteries' voltage dynamics are orders of magnitude slower than the power electronics control bandwidth, so the battery can be controlled to resemble a constant power source even as its voltage changes. Thus, the effectiveness of a BESS's response to short-term frequency events depends little on battery chemistry and heavily on the power electronics interface control design.

ACKNOWLEDGMENT

This work was supported primarily by the Engineering Research Center Program of the National Science Foundation and the Department of Energy under NSF Award Number EEC-1041877 and the CURENT Industry Partnership Program.

REFERENCES

[1] M. Aneke and M. Wang, "Energy storage technologies and real life applications – A state of the art review," *Applied Energy*, vol. 179, pp. 350–377, Oct. 2016.

[2] M. T. Lawder, B. Suthar, P. W. Northrop, S. De, C. M. Hoff, O. Leitermann, M. L. Crow, S. Santhanagopalan, and V. R. Subramanian, "Battery energy storage system (BESS) and battery management system (BMS) for grid-scale applications," *Proceedings of the IEEE*, vol. 102, no. 6, pp. 1014–1030, May 2014.

[3] "Grid energy storage," US Department of Energy, Tech. Rep., Dec. 2013.

[4] S. Sabihuddin, A. E. Kiprakis, and M. Mueller, "A numerical and graphical review of energy storage technologies," *Energies*, vol. 8, no. 1, pp. 172–216, Dec. 2014.

[5] A. Gallo, J. Simões-Moreira, H. Costa, M. Santos, and E. M. dos Santos, "Energy storage in the energy transition context: A technology review," *Renewable and Sustainable Energy Reviews*, vol. 65, pp. 800–822, Nov. 2016.

[6] D. M. Rastler, "Electricity energy storage technology options: A white paper primer on applications, costs and benefits," Electric Power Research Institute, Tech. Rep. 1020676, Dec. 2010.

[7] H. Verma, J. Gambhir, and S. Goyal, "Energy storage: A review," *International Journal of Innovative Technology and Exploring Engineering*, vol. 3, no. 1, Jun. 2013.

[8] J. D. Boles, "Battery energy storage emulation for power systems applications," Master's Thesis, University of Tennessee, Aug. 2017.

[9] A. Malhotra, B. Battke, M. Beuse, A. Stephan, and T. Schmidt, "Use cases for stationary battery technologies: A review of the literature and existing projects," *Renewable and Sustainable Energy Reviews*, vol. 56, pp. 705–721, Apr. 2016.

[10] (2017) U.S. energy storage monitor. Greentech Media. [Online]. Available: https://www.greentechmedia.com/research/subscription/u.s.-energy-storage-monitor

[11] A. A. Akhil, G. Huff, A. B. Currier, B. C. Kaun, D. M. Rastler, S. B. Chen, A. L. Cotter, D. T. Bradshaw, and W. D. Gauntlett, "DOE/EPRI 2013 electricity storage handbook in collaboration with NRECA," Sandia National Laboratories, Tech. Rep. SAND2013-5131, Jul. 2013.

[12] R. Kempener and E. Borden, "Battery storage for renewables: Market status and technology outlook," International Renewable Energy Agency, Tech. Rep., Jan. 2015.

[13] V. Knap, R. Sinha, M. Swierczynski, D.-I. Stroe, and S. Chaudhary, "Grid inertial response with lithium-ion battery energy storage systems," in *Proc. IEEE International Symposium on Industrial Electronics*, Istanbul, Turkey, Jun. 2014, pp. 1817–1822.

[14] J. Schmutz, "Primary frequency control provided by battery," Jun. 2013, Power Systems and High Voltage Laboratories, Federal Institute of Technology Zurich.

[15] B. Xu, A. Oudalov, J. Poland, A. Ulbig, and G. Andersson, "BESS control strategies for participating in grid frequency regulation," in *IFAC World Congress Proceedings Volumes*, vol. 47, no. 3, Aug. 2014, pp. 4024–4029.

[16] E. Thorbergsson, V. Knap, M. Swierczynski, D. Stroe, and R. Teodorescu, "Primary frequency regulation with li-ion battery based energy storage system - evaluation and comparison of different control strategies," in *Proc. International Telecommunications Energy Conference*, Hamburg, Germany, Oct. 2013, pp. 1–6.

[17] S. M. Alhejaj and F. M. Gonzalez-Longatt, "Impact of inertia emulation control of grid-scale BESS on power system frequency response," in *Proc. IEEE International Conference for Students on Applied Engineering*, Newcastle upon Tyne, United Kingdom, Oct. 2016, pp. 254–258.

[18] I. Serban and C. Marinescu, "Control strategy of three-phase battery energy storage systems for frequency support in microgrids and with uninterrupted supply of local loads," *IEEE Transactions on Power Electronics*, vol. 29, no. 9, pp. 5010–5020, Sep. 2014.

[19] J. Servotte, E. Acha, and L. M. Castro, "Smart frequency control in power transmission systems using a BESS," in *Proc. IEEE Innovative Smart Grid Technologies - Asia*, Bangkok, Thailand, Nov. 2015, pp. 1–7.

[20] S. J. Lee, J. H. Kim, C. H. Kim, S. K. Kim, E. S. Kim, D. U. Kim, K. K. Mehmood, and S. U. Khan, "Coordinated control algorithm for distributed battery energy storage systems for mitigating voltage and frequency deviations," *IEEE Transactions on Smart Grid*, vol. 7, no. 3, pp. 1713–1722, May 2016.

[21] "Balancing and frequency control," North American Electric Reliability Corporation (NERC) Resources Subcommittee, Tech. Rep., Jan. 2011.

[22] P. Tielens and D. Van Hertem, "Grid inertia and frequency control in power systems with high penetration of renewables," in *Proc. Young Researchers Symposium in Electrical Power Engineering*, Delft, The Netherlands, Apr. 2012.

[23] S. M. Alhejaj and F. M. Gonzalez-Longatt, "Investigation on grid-scale BESS providing inertial response support," in *Proc. IEEE International Conference on Power System Technology*, Wollongong, NSW, Australia, Sep. 2016, pp. 1–6.

[24] J. D. Boles, Y. Ma, W. Cao, L. M. Tolbert, and F. Wang, "Battery energy storage emulation in a converter-based power system emulator," in *Proc. IEEE Applied Power Electronics Conference and Exposition*, Tampa, FL, USA, Mar. 2017, pp. 2355–2362.

[25] J. Wang, L. Yang, Y. Ma, X. Shi, X. Zhang, L. Hang, K. Lin, L. M. Tolbert, F. Wang, and K. Tomsovic, "Regenerative power converters representation of grid control and actuation emulator," in *Proc. IEEE Energy Conversion Congress and Exposition*, Raleigh, NC, USA, Sep. 2012, pp. 2460–2465.

[26] L. Yang, X. Zhang, Y. Ma, J. Wang, L. Hang, K. Lin, L. M. Tolbert, F. Wang, and K. Tomsovic, "Hardware implementation and control design of generator emulator in multi-converter system," in *Proc. IEEE Applied Power Electronics Conference and Exposition*, Long Beach, CA, USA, Mar. 2013, pp. 2316–2323.

[27] L. Yang, Y. Ma, J. Wang, J. Wang, X. Zhang, L. M. Tolbert, F. Wang, and K. Tomsovic, "Development of converter based reconfigurable power grid emulator," in *Proc. IEEE Energy Conversion Congress and Exposition*, Pittsburgh, PA, USA, Sep. 2014, pp. 3990–3997.

[28] L. Yang, J. Wang, Y. Ma, J. Wang, X. Zhang, L. Tolbert, F. Wang, and K. Tomsovic, "Three-phase power converter based real-time synchronous generator emulation," *IEEE Transactions on Power Electronics*, vol. 32, no. 2, pp. 1651–1665, Feb. 2017.

[29] J. Wang, L. Yang, Y. Ma, J. Wang, L. M. Tolbert, F. F. Wang, and K. Tomsovic, "Static and dynamic power system load emulation in a converter-based reconfigurable power grid emulator," *IEEE Transactions on Power Electronics*, vol. 31, no. 4, pp. 3239–3251, Apr. 2016.

[30] W. Cao, Y. Ma, J. Wang, L. Yang, J. Wang, F. Wang, and L. M. Tolbert, "Two-stage PV inverter system emulator in converter based power grid emulation system," in *Proc. IEEE Energy Conversion Congress and Exposition*, Denver, CO, USA, Sep. 2013, pp. 4518–4525.

[31] Y. Ma, L. Yang, J. Wang, F. Wang, and L. M. Tolbert, "Emulating full-converter wind turbine by a single converter in a multiple converter based emulation system," in *Proc. IEEE Applied Power Electronics Conference and Exposition*, Fort Worth, TX, USA, Mar. 2014, pp. 3042–3047.

[32] R. Hidalgo-León and P. Jácome-Ruiz, "A survey on technologies to implement battery emulators based on DC/DC power converters." in *Proc. LACCEI International Multi-Conference for Engineering, Education, and Technology*, San José, Costa Rica, Jul. 2016, pp. 1–11.

[33] M. Michalczuk, B. Ufnalski, L. M. Grzesiak, and P. Rumniak, "Power converter-based electrochemical battery emulator," *Przeglad Elektrotechniczny*, vol. 90, no. 7, pp. 18–22, 2014.

[34] T. Mesbahi, N. Rizoug, P. Bartholomeus, and P. Le Moigne, "Li-ion battery emulator for electric vehicle applications," in *Proc. IEEE Vehicle Power and Propulsion Conference*, Beijing, China, Oct. 2013, pp. 2355–2362.

[35] O. König, G. Gregorčič, and S. Jakubek, "Model predictive control of a DC–DC converter for battery emulation," *Control Engineering Practice*, vol. 21, no. 4, pp. 428–440, Apr. 2013.

[36] A. Seaman, T.-S. Dao, and J. McPhee, "A survey of mathematics-based equivalent-circuit and electrochemical battery models for hybrid and electric vehicle simulation," *Journal of Power Sources*, vol. 256, pp. 410–423, Jun. 2014.

[37] A. R. Sparacino, G. F. Reed, R. J. Kerestes, B. M. Grainger, and Z. T. Smith, "Survey of battery energy storage systems and modeling techniques," in *Proc. IEEE Power and Energy Society General Meeting*, San Diego, CA, USA, Jul. 2012, pp. 1–8.

[38] Y. Cao, R. C. Kroeze, and P. T. Krein, "Multi-timescale parametric electrical battery model for use in dynamic electric vehicle simulations," *IEEE Transactions on Transportation Electrification*, vol. 2, no. 4, pp. 432–442, Dec. 2016.

[39] Y. Zhang, J. Zhao, P. Wang, M. Skyllas-Kazacos, B. Xiong, and R. Badrinarayanan, "A comprehensive equivalent circuit model of all-vanadium redox flow battery for power system analysis," *Journal of Power Sources*, vol. 290, pp. 14–24, Sep. 2015.

[40] M. Mohamed, H. Ahmad, M. A. Seman, S. Razali, and M. Najib, "Electrical circuit model of a vanadium redox flow battery using extended kalman filter," *Journal of Power Sources*, vol. 239, pp. 284–293, Oct. 2013.